

# GraphFusion3D: Dynamic Graph Attention Convolution with Adaptive Cross-Modal Transformer for 3D Object Detection

Md Sohag Mia<sup>1</sup>, Md Nahid Hasan<sup>2</sup>, Tawhid Ahmed<sup>2</sup>, Muhammad Abdullah Adnan<sup>2\*</sup>

<sup>1</sup>Nanjing University of Information Science and Technology, Nanjing, China

<sup>2</sup>Bangladesh University of Engineering and Technology, Dhaka, Bangladesh

shuvo2018@nuist.edu.cn, {0422052047, 0422052116, adnan}@cse.buet.ac.bd

## Abstract

*Despite significant progress in 3D object detection, point clouds remain challenging due to sparse data, incomplete structures, and limited semantic information. Capturing contextual relationships between distant objects presents additional difficulties. To address these challenges, we propose GraphFusion3D, a unified framework combining multi-modal fusion with advanced feature learning. Our approach introduces the Adaptive Cross-Modal Transformer (ACMT), which adaptively integrates image features into point representations to enrich both geometric and semantic information. For proposal refinement, we introduce the Graph Reasoning Module (GRM), a novel mechanism that models neighborhood relationships to simultaneously capture local geometric structures and global semantic context. The module employs multi-scale graph attention to dynamically weight both spatial proximity and feature similarity between proposals. We further employ a cascade decoder that progressively refines detections through multi-stage predictions. Extensive experiments on SUN RGB-D (70.6% AP<sub>25</sub> and 51.2% AP<sub>50</sub>) and ScanNetV2 (75.1% AP<sub>25</sub> and 60.8% AP<sub>50</sub>), demonstrate a substantial performance improvement over existing approaches.*

## 1. Introduction

Recently, 3D object detection from point clouds has become increasingly popular. As a core technique for 3D scene understanding, it is being utilized in many fields, such as domestic robotics, autonomous vehicles, and augmented reality. Accurate 3D detection is crucial for these applications because it enables machines to interact safely and intelligently with real-world environments, which are inherently three-dimensional. For example, autonomous vehicles rely on precise 3D perception to detect pedestrians, other vehicles, and road structures in complex, dy-

namic conditions. Similarly, service robots operating in indoor environments must be able to understand object shapes and positions to grasp or navigate around them reliably. These detection methods can be broadly categorized into two groups: 3D convolution-based approaches and voting-based approaches. Voting-based methods [16] cluster features via proposals but scale poorly when dealing with large point clouds due to high computational costs and the need for multiple passes over the data. Sparse 3D convolutions use voxels for efficient, scalable processing without losing density, enabling models to handle high-resolution point clouds with fewer resources. While most 3D models rely on point clouds, integrating multi-modal data [17], such as combining RGB images with LiDAR or depth scans, enhances detection accuracy by supplementing sparse geometry with rich semantic cues like texture and color. Some approaches depend solely on image data [10, 21]. While images offer rich color, texture, and semantic details, their lack of depth data limits their ability to predict precise 3D bounding boxes for 3D detection tasks. Some approaches depend solely on point clouds [11, 13, 14, 16], but point clouds are often irregular, sparse, and unordered, with varying point densities that may result in missing details, especially for small or distant objects. Small objects often get removed from the point cloud data, which can lead to blind regions and inaccurate scene representation. Information provided by the two different types of datasets is not similar to each other; rather, they complement each other, making multi-modal fusion a promising direction for robust perception. Recent research works focus on this limitation by utilizing both types of datasets [7, 15, 17, 27], combining geometric and semantic information to produce more accurate and complete 3D detections. These models can utilize both features, which in this case improves accuracy and robustness against occlusion and missing data. In order to capture the image features, ImVoteNet [17] utilizes a faster RCNN model, and EPNet++ [7] utilizes an encoder-decoder model with convolutional blocks.

Our proposed method advances 3D object detection

\*Corresponding auhtor

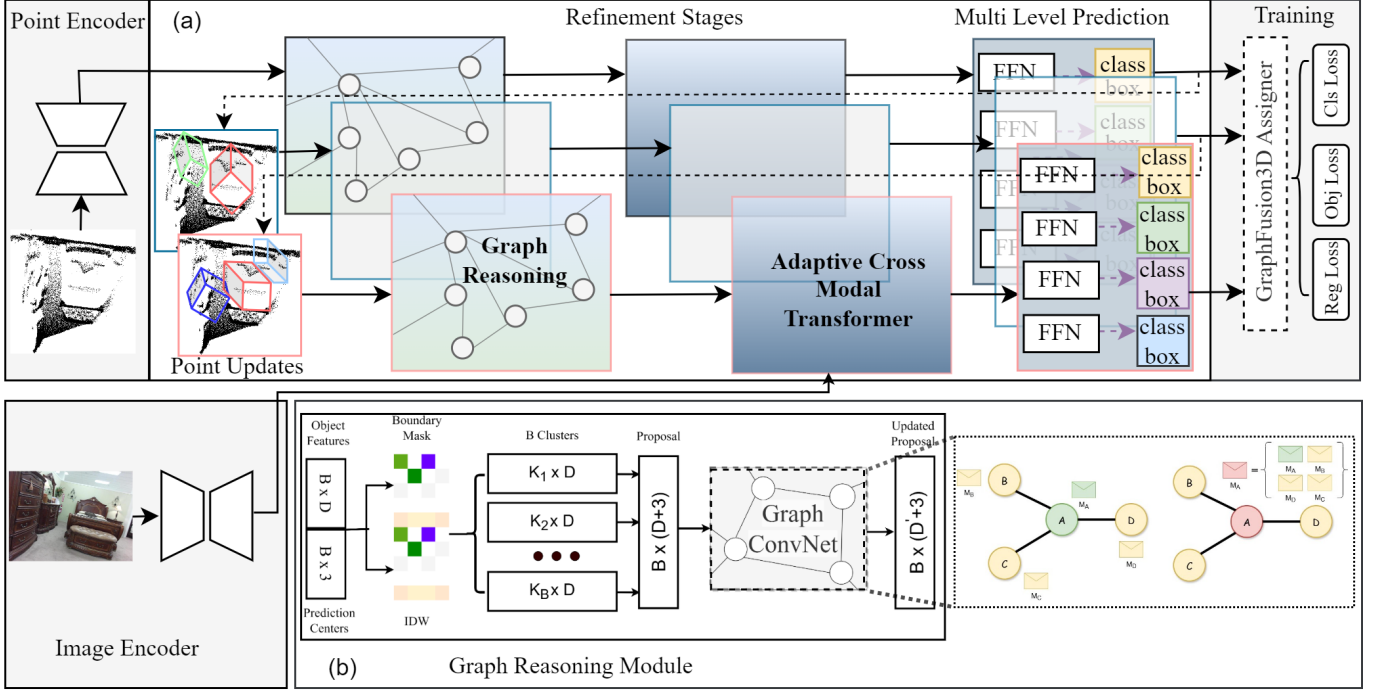


Figure 1. **Our proposed GraphFusion3D architecture.** The framework processes point clouds and RGB images through four key stages: (1) feature extraction via point and image backbone networks, (2) contextual refinement using the Graph Reasoning module, (3) multi-modal fusion via Adaptive Cross-Modal Transformer, and (4) progressive Cascade Refinement Decoding. Final detections are generated after multi-stage refinement.

through several key innovations. We employ Deform-DETR to extract discriminative image features from RGB inputs while developing a novel Graph reasoning module that enriches proposal features with neighborhood context. The framework incorporates a customized Deformable Feature Fusion module that dynamically aligns and combines multi-modal features from both point clouds and images. Further refinement is achieved through a cascade decoding process that progressively improves detection quality across multiple stages. Together, these components demonstrate the effectiveness of hybrid architectures for high-performance 3D perception in complex environments. Our overall work can be summarized as follows:

- We introduce a novel Graph Reasoning for Proposal Context, a multi-scale learnable graph module that captures semantic and geometric relations among image-point proposals.
- We propose an Adaptive Cross-Modal Transformer (ACMT), which dynamically aligns 2D image features and 3D point features in a context-aware manner, enabling effective image–point fusion and enriching both geometric and semantic representations for robust 3D object detection.
- Finally, we design a Progressive Cascaded Refinement Decoder, which iteratively refines detection proposals in

a cascaded manner, improving both accuracy and localization.

## 2. Related Work

We contextualize our approach within 3D object detection research, focusing on data modalities and architectural paradigms. Current methods primarily employ either point clouds or multi-modal inputs, implemented through voting, expansion, or transformer frameworks. While point-based approaches capture precise geometry, they often lack semantic richness—a limitation addressed by multi-modal methods through RGB fusion. This section reviews these critical developments.

### 2.1. Point Clouds Based

PointNet [13] processes irregular point sets via T-Net transformations and MLPs, extracting global features for detection. PointNet++ [14] extends the original PointNet by capturing local geometric structures through a hierarchical network that learns features at multiple scales for more robust 3D point cloud understanding. VoteNet [16] demonstrates how combining deep point set learning with Hough voting effectively addresses the challenge of detecting objects directly in sparse point clouds. It shows that strong 3D detection performance can be achieved us-

ing purely geometric information, without depending on 2D image data. GroupFree [9] leverages a transformer to progressively update object queries and integrate iterative predictions for refined 3D detection. 3DETR [11] brought an end-to-end transformer approach to the 3D detection of point clouds. The class-aware grouping strategy together with sparse convolutional RoI pooling in CAGroup3D [24] leads to better 3D object detection results on ScanNet and SUN RGB-D benchmarks with improved accuracy and efficiency. The Vertex Relative Position Encoding (3DV-RPE) method in V-DETR [20] boosts 3D object detection performance through attention mechanisms that focus on spatially related points according to the locality principle. The technique obtains leading performance results for ScanNetV2 by surpassing CAGroup3D with significant improvement. SPGroup3D [29] utilizes superpoint grouping methods which integrate geometry-based voting together with feature fusion to achieve better semantic matching and precise one-stage 3D object detection for indoor environments. UniDet3D [6] solves the problem of dataset-dependant 3D object detectors by bringing together multiple indoor datasets using a common label system which results in enhanced model robustness and generalization capabilities. Through its transformer architecture the system delivers notable performance improvements on six key benchmarks which proves its suitability for multiple indoor use cases. SOFW [4] presents a unified framework which optimizes indoor 3D object detection across multiple datasets through simultaneous domain parameter optimization between shared and specific domains while maintaining model complexity at a constant level.

## 2.2. Multi-Modal Based

The ImVoteNet [17] system improves VoteNet through its integration of 2D visual and 3D point cloud data, which solves missing information problems in point clouds. The system integrates two independent backbones along with specialized towers which enhance multi-modal fusion capabilities for detection. The method [22] merges 3D CNN depth feature representations with 2D VGG color outputs by combining them through concatenation to perform SUN RGB-D [23] 3D detection. By integrating RGB and point clouds through transformers, TokenFusion [25] dynamically replaces low-information tokens in one modality with fused cross-modal features, boosting accuracy in geometrically or texturally ambiguous regions. EPNet++ [7] model merges RGB and point cloud data at intermediate backbone layers, refining cross-modal alignment through progressive feature fusion. [27] Employs dual pipelines for image and point cloud data, using a DeMF module to fuse object-level visual information into point features, but skips the feature refinement process. MTC-RCNN [12] cascades a 3D detection framework with intermediate 2D segmentation,

leveraging pixel-level semantics to improve proposal refinement. FCAF3D [18] implements full convolutional anchor-free detection through point-based proposal parametrization but faces challenges with irregular geometries because noisy coarse proposal points do not align properly with ground truth centers. TR3D [19] introduces a lightweight fully-convolutional 3D object detector that enhances sparse CNNs for better accuracy and efficiency and its TR3D+FF version uses early fusion of RGB and point cloud features to deliver state-of-the-art multimodal performance.

## 3. THE PROPOSED METHOD

In this section, we present our proposed framework for 3D object detection, illustrated in Fig. 1. Our approach consists of three key components: (1) a Graph-Aware Voting Mechanism, which enhances proposal features by leveraging neighborhood context; (2) a Adaptive Cross-Modal Alignment (ACMT) Mechanism, which effectively integrates multi-modal data from images and point clouds; and (3) Progressive Cascaded Refinement Decoder, designed to progressively refine detection outputs; Below, we detail each component in sequence.

### 3.1. Graph Reasoning Module

We propose a novel Graph Reasoning Module (GRM) that models both geometric and semantic relationships among proposals via multi-scale graph attention convolutional networks (depicted in Fig. 1(b)). The GRM explicitly encodes contextual dependencies, leveraging the fact that certain spatial configurations recur in indoor layouts (e.g., chairs near tables, beds beside nightstands). This module integrates three key operations: boundary-aware feature aggregation, multi-scale attention-based graph convolution, and residual fusion.

The first stage performs *boundary-aware feature aggregation* using conditional inverse distance weighting (IDW), ensuring that features are aggregated only from spatially relevant regions:

$$f_i = \frac{\sum_{j \in \mathcal{N}(i)} \zeta_{i,j} w_{i,j} f_j}{\sum_{j \in \mathcal{N}(i)} \zeta_{i,j} w_{i,j}}, \quad w_{i,j} = \exp\left(-\frac{\|p'_i - p_j\|}{\sigma}\right), \quad (1)$$

where  $p'_i$  is the proposal coordinate,  $f_j$  denotes neighboring point features,  $\zeta_{i,j}$  is a boundary mask, and  $\sigma$  is set to the mean  $k$ -NN distance to stabilize aggregation across variable densities. This normalization avoids bias from dense neighborhoods and ensures spatially consistent feature refinement.

Next, we construct an attention-based graph convolution that captures both geometric and feature-level dependencies:

$$e_{ij} = h_\varphi(x_i, x_j, p_i - p_j), \quad (2)$$

where  $h_\varphi$  is a nonlinear function with learnable parameters  $\varphi$ . Edge weights are computed from both feature similarity and spatial distance across three neighborhood scales  $k \in \{5, 10, 20\}$ :

$$w_{ij}^{(s)} = \exp\left(-\frac{\|p_i - p_j\|^2}{2\sigma_s^2}\right), \quad (3)$$

where  $\sigma_s$  represents the adaptive scale parameter derived from the mean distance to the  $k$ -th nearest neighbor, ensuring stable edge weight computation across varying point densities. These spatial weights are then combined with feature-based attention coefficients:

$$\alpha_{ij}^{(s)} = \frac{\exp(\text{sim}(q_i^{(s)}, k_j^{(s)}))}{\sum_{m \in \mathcal{N}_s(i)} \exp(\text{sim}(q_i^{(s)}, k_m^{(s)}))}. \quad (4)$$

where  $q_i^{(s)}$  and  $k_j^{(s)}$  are learnable query and key vectors derived from node features, and  $\text{sim}(\cdot, \cdot)$  denotes cosine similarity. This dual-weighting mechanism dynamically balances spatial proximity and feature relevance, allowing the model to focus on semantically important relationships while respecting geometric constraints.

The aggregated representation for each scale is then:

$$\tilde{f}_i^{(s)} = \sum_{j \in \mathcal{N}_s(i)} \alpha_{ij}^{(s)} w_{ij}^{(s)} \psi^{(s)}(e_{ij}^{(s)}), \quad (5)$$

followed by scale fusion and residual update:

$$f_i'' = f_i + \gamma \cdot \text{MLP}([\tilde{f}_i^{(5)}; \tilde{f}_i^{(10)}; \tilde{f}_i^{(20)}]), \quad (6)$$

where  $\gamma$  is a learnable scalar.

GRM is applied twice within the transformer decoder—once before decoding to establish a coarse relational context, and again after the first decoding stage for fine-grained relational refinement. This two-step reasoning enables both object-level and scene-level contextual understanding. GRM produces context-aware proposal relationships without relying on external segmentation, enabling seamless integration within the unified GraphFusion3D pipeline.

### 3.2. Adaptive Cross-Modal Transformer

The Adaptive Cross-Modal Transformer (ACMT) operates on the relationally structured proposals from GRM, using them as geometric anchors for its cross-modal attention. ACMT is the core fusion module in GraphFusion3D, designed to unify geometric information from 3D points and semantic cues from RGB images in a spatially consistent manner. ACMT alternates attention between the point-cloud and image modalities, guided by adaptive modality weighting through a *Cross-Modal Gating (CMG)* mechanism. This design allows the network to dynamically balance 2D and 3D cues depending on object scale, visibility, and context. The ACMT module is shown in Fig. 2.

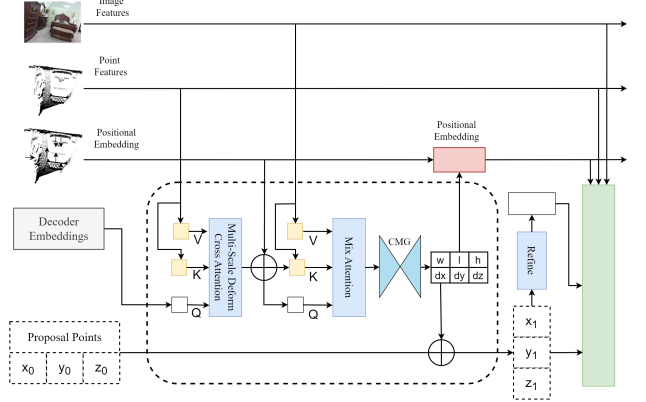


Figure 2. The architecture of the Adaptive Cross-Modal Transformer module.

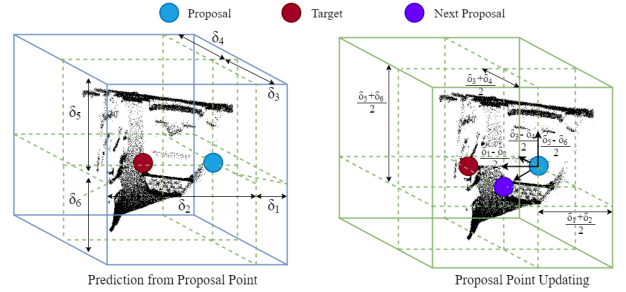


Figure 3. Illustration of a progressive cascaded refinement decoder module. Left: Bounding box from a single proposal point with predicted  $\delta$ . Right: Updating process from proposal point to bounding box center.

**Feature Extraction.** We employ a ResNet backbone to extract multi-scale image features  $\{x_i^l\}_{l=1}^L$  ( $L = 4$ ) and a sparse 3D convolutional encoder to obtain geometric features  $x^p \in \mathbb{R}^{N \times C}$ . The two feature streams are spatially aligned through explicit geometric projection.

Each 3D point  $\mathbf{P} = [x, y, z, 1]^\top$  in camera coordinates is projected onto the image plane using the intrinsic matrix  $\mathbf{K}$  and extrinsic parameters  $[\mathbf{R}|\mathbf{t}]$ :

$$\begin{bmatrix} \tilde{u} \\ \tilde{v} \\ \tilde{w} \end{bmatrix} = \mathbf{K}[\mathbf{R}|\mathbf{t}]\mathbf{P}, \quad (u, v) = \left( \frac{\tilde{u}}{\tilde{w}}, \frac{\tilde{v}}{\tilde{w}} \right).$$

The resulting coordinates  $(u, v)$  are then normalized to the range  $[0, 1]^2$  using the image dimensions:

$$\text{refPoint} = \left( \frac{u}{W_0}, \frac{v}{H_0} \right),$$

where  $W_0$  and  $H_0$  denote the image width and height, respectively. This normalization ensures consistent pixel-



level alignment between projected 3D points and 2D feature maps, allowing ACMT to sample semantically relevant regions during fusion.

**Cross-Modal Fusion.** Given the aligned features, ACMT performs alternating attention between modalities to refine object queries  $y$ . At each layer, point features  $x^p$  provide geometric priors through cross-attention, while image embeddings  $x^i$  contribute semantic detail through deformable attention:

$$\begin{aligned} y &= y + \text{CrossAttn}(y, x^p), \\ y &= y + \text{MSDeformAttn}(y, x^i), \\ y &= y + \text{FFN}(y), \end{aligned} \quad (7)$$

where CrossAttn models spatial dependencies in the 3D domain and MSDeformAttn selectively aggregates multi-scale image features around projected reference points. This formulation allows ACMT to reason jointly over geometric structure and visual appearance while maintaining computational efficiency.

**Cross-Modal Gating (CMG).** To adaptively balance geometric and visual cues, CMG predicts modality-specific weights conditioned on the current query context and both feature streams. Given query features  $y$ , point features  $y^p$ , and image features  $y^i$ , the gating network first concatenates them and passes the result through a multi-layer perceptron (MLP) with layer normalization and ReLU activation:

$$[\lambda_p, \lambda_i] = \text{Softmax}(\text{MLP}([y; y^p; y^i])),$$

where  $\lambda_p, \lambda_i \in \mathbb{R}^H$  correspond to per-head weights for point and image modalities, respectively. The fused representation is then computed as:

$$y' = \lambda_p \odot y^p + \lambda_i \odot y^i,$$

where  $\odot$  denotes element-wise weighting across attention heads. This fine-grained gating mechanism dynamically adjusts the contribution of each modality, emphasizing geometric structure when appearance cues are unreliable and amplifying semantic detail when visual context is strong. ACMT integrates the gating mechanism directly within the transformer layers rather than using it as an external weighting step. This joint formulation enables context-aware reweighting at every fusion stage and stabilizes gradient flow between 2D and 3D branches. The result is a more robust cross-modal alignment capable of handling complex indoor scenes with partial observations.

### 3.3. Progressive Cascaded Refinement Decoder

Using the relational-semantic features produced by ACMT, the Progressive Cascaded Refinement Decoder updates box geometry in a multi-stage fashion. The Progressive Cascaded Refinement Decoder iteratively improves proposal localization and feature quality through multi-stage refinement. Given initial proposals  $(\mathbf{x}^p, \mathbf{p})$ , each stage predicts

box offsets  $\delta = \{\delta_1, \dots, \delta_6\}$  relative to the ground-truth box  $\mathbf{g} = (x, y, z, w, l, h, \theta)$ :

$$\begin{aligned} \delta_1 &= x + \frac{w}{2} - \hat{x}, & \delta_2 &= \hat{x} - x + \frac{w}{2}, \\ \delta_3 &= y + \frac{l}{2} - \hat{y}, & \delta_4 &= \hat{y} - y + \frac{l}{2}, \\ \delta_5 &= z + \frac{h}{2} - \hat{z}, & \delta_6 &= \hat{z} - z + \frac{h}{2}. \end{aligned} \quad (8)$$

To bring proposals closer to ground truth centers, the decoder updates the 3D coordinates at each stage as:

$$\hat{x}' = \hat{x} + \frac{\delta_1 - \delta_2}{2}, \quad \hat{y}' = \hat{y} + \frac{\delta_3 - \delta_4}{2}, \quad \hat{z}' = \hat{z} + \frac{\delta_5 - \delta_6}{2}.$$

Centerness supervision encourages points closer to the true object center. Let the centerness target  $\hat{c}^*$  be defined based on the normalized regression targets  $\delta^*$  as:

$$\hat{c}^* = \prod_{i=1}^3 \frac{\min(\delta_{2i-1}^*, \delta_{2i}^*)}{\max(\delta_{2i-1}^*, \delta_{2i}^*)}.$$

A point is assigned positive if it lies within the ground-truth spatial region, reducing noise from distant samples. Updating process is shown in Fig. 3.

**GraphFusion3D Assigner.** Existing assigners [18, 19] often fail with thin objects or sparse point distributions due to strict boundary constraints. Our GraphFusion3D Assigner overcomes this by combining boundary-aware matching with cascade threshold scheduling. It progressively decreases the positive assignment threshold across decoder stages while considering points both inside and near bounding boxes, ensuring abundant training samples initially and high-quality positives later for challenging objects.

**Training Objective.** The final optimization combines classification, regression, and centerness losses:

$$\mathcal{L} = \lambda_{\text{cls}} \mathcal{L}_{\text{cls}} + \lambda_{\text{reg}} \mathcal{L}_{\text{reg}}^{\text{RotatedIoU3D}} + \lambda_{\text{ctr}} \mathcal{L}_{\text{ctr}},$$

with  $\lambda_{\text{cls}}=1.0$ ,  $\lambda_{\text{reg}}=2.0$ ,  $\lambda_{\text{ctr}}=1.0$ . This balanced loss design stabilizes training and ensures accurate 3D localization and class prediction across refinement stages.

## 4. EXPERIMENTS

### 4.1. Datasets and Evaluation Metrics

**Datasets.** We conduct experiments on two standard indoor benchmarks: SUN RGB-D [23] and ScanNetv2 [3]. **(a) SUN RGB-D** consists of 10,335 RGB-D images annotated with oriented 3D bounding boxes across 37 categories. Following VoteNet, we evaluate on the 10 most frequent categories using the official train/val split (5,285 / 5,050 samples). **(b) ScanNetv2** contains 1,513 reconstructed 3D indoor scenes with per-point semantic and instance annotations across 18 object categories, divided into 1,201 training and 312 validation scans.

**Evaluation Metric.** For all datasets, we use mean average precision (AP) at IoU thresholds of 0.25 and 0.5, the same

Methods	Modal	Bed	Table	Sofa	Chair	Toilet	Desk	Dresser	Stand	Shelf	Tub	AP <sub>25</sub>	AP <sub>50</sub>
VoteNet [16]	P	83.0	47.3	64.0	75.3	90.1	22.0	29.8	62.2	28.8	74.4	57.7	
3DETR [11]	P	81.8	50.0	58.3	68	90.3	28.7	28.6	56.6	27.5	77.6	59.1	32.7
GroupFree [9]	P	87.8	53.8	70.0	79.4	91.1	32.6	36.0	66.7	32.5	80.0	63.0	45.2
FCAF3D [18]	P	87.6	53.6	70.7	81.5	92.3	37.1	39.8	70.2	34.5	80.1	64.2	48.9
HGNet [1]	P	84.5	51.6	65.7	75.2	91.1	34.3	37.6	61.7	35.7	78.0	61.6	
TR3D [19]	P	88.7	58.5	71.8	82.8	92.9	41.7	44.8	73.1	36.3	78.4	67.1	50.4
SPGroup3D [29]	P	89.6	55.9	74.9	81.0	90.3	38.6	37.8	66.4	38.1	78.6	65.4	47.1
CAGroup3D [24]	P	89.1	59.6	73.6	83.9	91.7	40.6	40.5	72.9	35.4	82.6	66.8	50.2
V-DETR [20]	P											67.5	50.4
Uni3DETR [26]	P											67.0	50.3
MMTC [12]	P+I	86.3	54.4	68.2	79.7	92.8	29.7	47.2	69.5	46.3	78.8	65.3	48.6
TR3D+FF [19]	P+I											69.4	53.4
EPNet++ [7]	P+I	89.1	51.3	71.9	80.2	92.4	32.5	45.2	67.4	47.1	76.3	65.3	
TokenFusion [25]	P+I											64.9	48.3
ImVoteNet [17]	P+I	87.6	51.1	70.7	76.7	90.5	28.7	41.4	69.9	41.3	75.9	64.4	43.3
GraphFusion3D	P	86.1	53.7	69.3	80.3	92.7	36.1	39.3	70.2	34.0	78.2	64.0	47.1
GraphFusion3D	P+I	92.5	62.1	78.8	86.5	92.8	48.9	45.7	82.0	31.7	84.0	70.6	51.2

Table 1. State-of-the-art results comparison of each object, AP<sub>25</sub> and AP<sub>50</sub> on SUN RGB-D. P= Point only input, and P+I= Point + RGB inputs.

Methods	Modal	AP <sub>25</sub>	AP <sub>50</sub>
VoteNet	P	58.6	33.5
3DETR	P	65.0	47.0
FCAF3D	P	71.5	57.3
SPGroup3D	P	74.3	59.6
Uni3DETR	P	71.7	58.3
CAGroup3D	P	75.1	61.3
UniDet3D	P	77.5	66.1
TR3D	P	72.9	59.3
V-DETR	P	77.4	65.0
GraphFusion3D	P	72.8	57.9
GraphFusion3D	P+I	75.1	60.8

Table 2. Quantitative evaluation on ScanNetV2. P= Point only input, and P+I= Point + RGB inputs.

Backbones	Point backbone	Image backbone	AP <sub>25</sub>	AP <sub>50</sub>
CNNs	MinkResNet34	ResNet	70.6	51.2
Transformers	Swin3D	Swin-T	71.8	52.6

Table 3. Effect of different backbones on SUNRGB-D dataset.

as VoteNet. To ensure reliability, We train each model five times and evaluate each trained model five times independently. For comparison, we report the best results obtained across all runs.

## 4.2. Implementation Details

Our implementation follows standard 3D detection pipelines [18]. We uniformly sample  $N = 100,000$  points

Module	Params (M)	FPS	AP <sub>25</sub>	AP <sub>50</sub>
Baseline	103.7	16.39	64.0	47.1
+ ACMT	124.6	12.76	67.3	49.2
+ CRD	124.6	10.18	68.4	49.4
+ GRM	126.2	10.01	70.6	51.2

Table 4. Performance impact of different modifications on SUN RGBD and module-wise runtime and parameter breakdown of GraphFusion3D.

per scene with a voxel size of 0.01 and employ a single set aggregation for proposal generation. Each proposal is iteratively refined through bounding-box regression and classification branches. The model is trained for 12 epochs using the AdamW optimizer with an initial learning rate of  $1 \times 10^{-4}$ , decayed by 0.1 at the 8th and 11th epochs. We apply a weight decay of 0.01 and use a batch size of 4 on a single NVIDIA RTX 4090 GPU. Losses are jointly applied at proposal and final prediction stages to stabilize training.

## 4.3. Comparisons with State-of-the-Art

We evaluate GraphFusion3D on two different datasets. On SUN RGB-D benchmark, with results summarized in Table 1. Our model achieves 70.6 AP<sub>25</sub> and 51.2 AP<sub>50</sub>, surpassing recent state-of-the-art 3D detection frameworks such as V-DETR (67.5 AP<sub>25</sub>), Uni3DETR (67.0 AP<sub>25</sub>), TR3D+FF (69.4 AP<sub>25</sub>), and CAGroup3D (66.8 AP<sub>25</sub>). GraphFusion3D attains notable category-level gains for challenging classes like chairs, sofas, and beds, highlighting its effectiveness in modeling both detailed geometric struc-

Setting	$k$	AP <sub>25</sub>	AP <sub>50</sub>
No Graph Reasoning	—	68.4	49.4
Single-Scale (Local)	5	68.6	49.5
Single-Scale (Mid-range)	10	68.9	50.0
Single-Scale (Global)	20	69.8	50.4
Multi-Scale ( $k=5,10,20$ )	All	<b>70.6</b>	<b>51.2</b>

Table 5. Ablation study on the Graph Reasoning module with different neighborhood scales  $k$  on SUN RGB-D. Multi-scale fusion shows the strongest performance by combining complementary local, mid-range, and global contexts.

Decoder Stages	SUNRGB-D		ScanNetV2	
	AP <sub>25</sub>	AP <sub>50</sub>	AP <sub>25</sub>	AP <sub>50</sub>
Single-stage (Baseline)	69.5	50.9	73.9	59.6
Two-stage	70.4	51.1	74.8	60.5
Full Cascade (Three-stage)	70.6	51.2	75.1	60.8

Table 6. Effect of different cascaded stages.

Fusion Variant	SUNRGB-D		ScanNetV2	
	AP <sub>25</sub>	AP <sub>50</sub>	AP <sub>25</sub>	AP <sub>50</sub>
w/o Cross-Modal Gating	70.3	50.6	74.7	59.9
w/ Cross-Modal Gating	70.6	51.2	75.1	60.8

Table 7. Ablation study of the Adaptive Cross-Modal Transformer.

tures and global scene context. These improvements arise from the synergy between the Graph Reasoning and Adaptive Cross-Modal Transformer modules, which together enhance spatial reasoning and image-point alignment. On ScanNetV2, our multimodal model (P+I) achieves 75.1 AP<sub>25</sub> and 60.8 AP<sub>50</sub> (Table 2). While these results demonstrate the effectiveness of our fusion approach, they do not reach the current state-of-the-art for this dataset. This is primarily because our method is specifically optimized for multimodal fusion, and we used only 10 multi-view images per scan during training—significantly fewer than the 200+ views available in the original dataset. This limitation in visual data coverage constrained our model’s ability to fully exploit the complementary RGB information available in ScanNetV2. Nevertheless, the consistent improvement over our point-only variant (72.8 AP<sub>25</sub>) validates the benefits of our cross-modal fusion design. Fig. 4 and Fig. 5 present qualitative detection results on ScanNetV2 and SUN RGB-D, respectively.

#### 4.4. Efficiency and Complexity Analysis

We analyze the efficiency of our proposed modules in Table 4. The baseline model achieves 64.0% AP<sub>25</sub> with 103.7M parameters. Incorporating the Adaptive

Cross-Modal Transformer (ACMT) increases parameters to 124.6M and improves AP<sub>25</sub> to 67.3%. Adding the Cascade Refinement Decoder (CRD) maintains the same parameter count while further boosting AP<sub>25</sub> to 68.4%. The full model with the Graph Reasoning Module (GRM) uses 126.2M parameters and achieves 70.6% AP<sub>25</sub>, demonstrating that significant performance gains are attained with only a moderate increase in model size. Despite the added complexity, our design maintains a competitive inference speed of 10.01 FPS.

#### 4.5. Ablation Studies

We perform extensive ablation studies on the SUN RGB-D and ScanNetV2 datasets to isolate the contribution of each core module in GraphFusion3D. All experiments use the same training protocol and evaluation setup for fairness.

**Impact of Adaptive Cross-Modal Transformer.** The Adaptive Cross-Modal Transformer (ACMT) strengthens image–point fusion through the proposed Cross-Modal Gating (CMG) mechanism, which dynamically regulates the contribution of geometric and visual features. Starting from the point-only baseline of 64.0 AP<sub>25</sub>, adding ACMT (without GRM and CRD) significantly improves performance to 67.3 AP<sub>25</sub> on SUN RGB-D (Table 4). CMG learns adaptive modality weights ( $\lambda_p, \lambda_i$ ) conditioned on each query representation, allowing the model to emphasize point-based geometry when visual cues are unreliable (e.g., occlusion or depth noise) and to rely more on image features when appearance information is strong. Without CMG, the baseline ACMT achieves 70.3 AP<sub>25</sub> and 50.6 AP<sub>50</sub> on SUNRGB-D and 74.7 AP<sub>25</sub> and 59.9 AP<sub>50</sub> on ScanNetV2, whereas incorporating CMG improves alignment and robustness to 70.6 AP<sub>25</sub> and 51.2 AP<sub>50</sub> on SUNRGB-D and 75.1 AP<sub>25</sub> and 60.8 AP<sub>50</sub> on ScanNetV2 (Table 7).

**Backbone Choice.** We also examine the impact of different backbone configurations (Table 3). Standard CNN backbones (MinkResNet34 [2] for point clouds and ResNet [5] for images) yield strong performance with 70.6 AP<sub>25</sub> and 51.2 AP<sub>50</sub>. Replacing them with transformer-based architectures (Swin3D [28] and Swin-T [8]) further improves performance to 71.8 AP<sub>25</sub> and 52.6 AP<sub>50</sub>, demonstrating enhanced context modeling and long-range reasoning. These results confirm that our fusion design generalizes effectively and benefits from the superior global dependency capture of transformers.

**Impact of Cascaded Refinement.** As shown in Table 6, our progressive cascade decoder consistently improves performance across both datasets. On SUN RGB-D, performance increases from 69.5 AP<sub>25</sub>/50.9 AP<sub>50</sub> (single-stage) to 70.4/51.1 (two-stage) and finally 70.6/51.2 (three-stage). Similarly, ScanNetV2 improves from 73.9/59.6 to 75.1/60.8. Each stage enhances box localization through iterative center refinement and feature updating, with dimin-

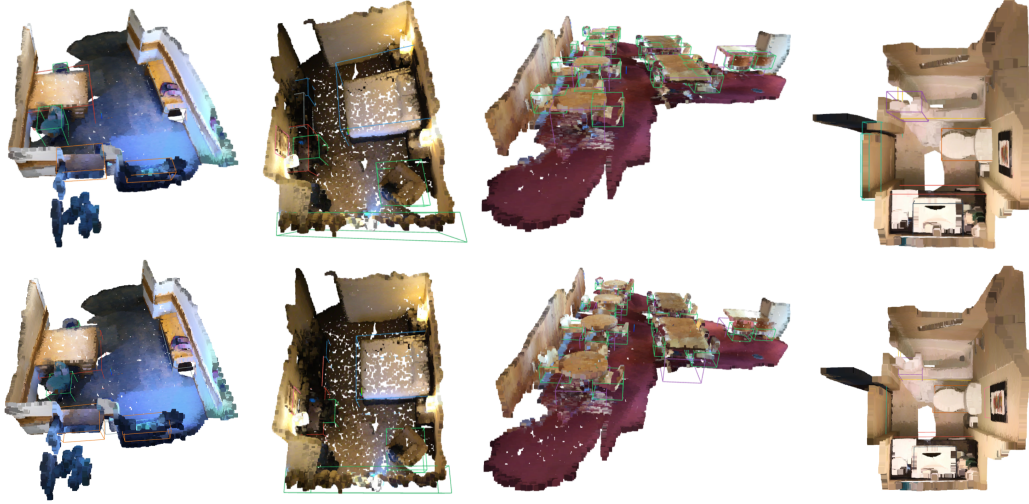


Figure 4. Qualitative prediction results on the ScanNetV2. The first row displays the ground-truth data, while the second row presents the detection results from our GraphFusion3D.



Figure 5. Qualitative prediction results on the SUN RGB-D. The first row displays the ground-truth data, while the second row presents the detection results from our GraphFusion3D.

ishing returns after the second stage.

**Graph Reasoning Module.** The proposed Graph Reasoning Module module contributes significant improvement, delivering a +2.2  $AP_{25}$  gain through explicit reasoning over spatial and semantic relationships between proposals. Unlike standard convolutional aggregation, GRM constructs a learnable graph where each proposal interacts with its neighbors across multiple receptive-field scales  $k = \{5, 10, 20\}$ . At each scale, edge affinities are computed by jointly considering spatial distance (via a Gaussian kernel) and feature similarity (via cosine attention), allowing the model to dynamically balance geometric proximity and semantic consistency. As shown in Table 5, smaller neighborhoods ( $k = 5$ ) enhance fine-grained details such as object parts, whereas larger neighborhoods ( $k = 20$ ) capture room-level spatial layouts. Integrating all scales yields

the best results 70.6  $AP_{25}$  and 51.2  $AP_{50}$ , demonstrating that hierarchical context aggregation is crucial for complex indoor scenes. This progressive multi-scale reasoning enables the detector to more accurately localize spatially correlated objects—such as chairs around tables or monitors on desks—while maintaining robustness to clutter and occlusion.

#### 4.6. Discussion of Limitations

While GraphFusion3D achieves strong multimodal performance, its point-only accuracy (72.8  $AP_{25}$  on ScanNetV2) lags behind specialized point-based methods. This limitation stems from our architecture’s optimization for cross-modal fusion, which underutilizes spatial-semantic correlations when image data is absent. Future work will enhance modality robustness to maintain performance with partial or missing visual inputs.

## 5. Conclusion

We presented GraphFusion3D, a unified framework for indoor 3D object detection that effectively fuses geometric and visual information. Our approach integrates three key components: an Adaptive Cross-Modal Transformer (ACMT) for dynamic image-point fusion, a Graph Reasoning Module (GRM) for contextual relationship modeling, and a Cascaded Refinement Decoder for progressive localization. Extensive experiments demonstrate that GraphFusion3D achieves state-of-the-art performance on the SUN RGB-D benchmark and competitive results on ScanNetV2, highlighting the effectiveness of our context-aware fusion and hierarchical reasoning for accurate and robust 3D detection in complex indoor scenes.



## References

- [1] Jintai Chen, Biwen Lei, Qingyu Song, Haochao Ying, Danny Z Chen, and Jian Wu. A hierarchical graph network for 3d object detection on point clouds. In *Proceedings of the IEEE/CVF conference on computer vision and pattern recognition*, pages 392–401, 2020. 6
- [2] Christopher Choy, JunYoung Gwak, and Silvio Savarese. 4d spatio-temporal convnets: Minkowski convolutional neural networks. In *Proceedings of the IEEE/CVF Conference on Computer Vision and Pattern Recognition (CVPR)*, 2019. 7
- [3] Angela Dai, Angel X Chang, Manolis Savva, Maciej Halber, Thomas Funkhouser, and Matthias Nießner. Scannet: Richly-annotated 3d reconstructions of indoor scenes. In *Proceedings of the IEEE conference on computer vision and pattern recognition*, pages 5828–5839, 2017. 5
- [4] Kun Dai, Zhiqiang Jiang, Tao Xie, Ke Wang, Dedong Liu, Zhendong Fan, Ruifeng Li, Lijun Zhao, and Mohamed Omar. Sofw: A synergistic optimization framework for indoor 3d object detection. *IEEE Transactions on Multimedia*, pages 637–651, 2025. 3
- [5] Kaiming He, Xiangyu Zhang, Shaoqing Ren, and Jian Sun. Deep residual learning for image recognition. In *Proceedings of the IEEE Conference on Computer Vision and Pattern Recognition (CVPR)*, 2016. 7
- [6] Maksim Kolodiaznyy, Anna Vorontsova, Matvey Skripkin, Danila Rukhovich, and Anton Konushin. Unidet3d: Multi-dataset indoor 3d object detection. In *Proceedings of the AAAI Conference on Artificial Intelligence*, pages 4365–4373, 2025. 3
- [7] Zhe Liu, Tengting Huang, Bingling Li, Xiwu Chen, Xi Wang, and Xiang Bai. Epnet++: Cascade bi-directional fusion for multi-modal 3d object detection. *IEEE Transactions on Pattern Analysis and Machine Intelligence*, 45: 8324–8341, 2021. 1, 3, 6
- [8] Ze Liu, Yutong Lin, Yue Cao, Han Hu, Yixuan Wei, Zheng Zhang, Stephen Lin, and Baining Guo. Swin transformer: Hierarchical vision transformer using shifted windows. In *Proceedings of the IEEE/CVF International Conference on Computer Vision (ICCV)*, pages 10012–10022, 2021. 7
- [9] Ze Liu, Zheng Zhang, Yue Cao, Han Hu, and Xin Tong. Group-free 3d object detection via transformers. In *Proceedings of the IEEE International Conference on Computer Vision*, pages 2929–2938. Institute of Electrical and Electronics Engineers Inc., 2021. 3, 6
- [10] Zongdai Liu, Dingfu Zhou, Feixiang Lu, Jin Fang, and Liangjun Zhang. AutoShape: Real-Time Shape-Aware Monocular 3D Object Detection. In *2021 IEEE/CVF International Conference on Computer Vision (ICCV)*, pages 15621–15630, Los Alamitos, CA, USA, 2021. 1
- [11] Ishan Misra, Rohit Girdhar, and Armand Joulin. An end-to-end transformer model for 3d object detection. In *Proceedings of the IEEE International Conference on Computer Vision*. Institute of Electrical and Electronics Engineers Inc., 2021. 1, 3, 6
- [12] Jinhyung Park, Xinshuo Weng, Yunze Man, and Kris Kitani. Multi-modality task cascade for 3d object detection. In *The British Machine Vision Conference (BMVC)*, 2021. 3, 6
- [13] Charles R. Qi, Hao Su, Kaichun Mo, and Leonidas J. Guibas. Pointnet: Deep learning on point sets for 3d classification and segmentation. In *Proceedings - 30th IEEE Conference on Computer Vision and Pattern Recognition, CVPR 2017*, pages 77–85. Institute of Electrical and Electronics Engineers Inc., 2016. 1, 2
- [14] Charles R Qi, Li Yi, Hao Su, and Leonidas J Guibas. Pointnet++: Deep hierarchical feature learning on point sets in a metric space. *arXiv preprint arXiv:1706.02413*, 2017. 1, 2
- [15] Charles R Qi, Wei Liu, Chenxia Wu, Hao Su, and Leonidas J Guibas. Frustum pointnets for 3d object detection from rgb-d data. In *Proceedings of the IEEE conference on computer vision and pattern recognition*, pages 918–927, 2018. 1
- [16] Charles R Qi, Or Litany, Kaiming He, and Leonidas J Guibas. Deep hough voting for 3d object detection in point clouds. In *proceedings of the IEEE/CVF International Conference on Computer Vision*, pages 9277–9286, 2019. 1, 2, 6
- [17] Charles R Qi, Xinlei Chen, Or Litany, and Leonidas J Guibas. Imvotenet: Boosting 3d object detection in point clouds with image votes. In *IEEE Conference on Computer Vision and Pattern Recognition (CVPR)*, 2020. 1, 3, 6
- [18] Danila Rukhovich, Anna Vorontsova, and Anton Konushin. Fcaf3d: Fully convolutional anchor-free 3d object detection. In *European Conference on Computer Vision*, pages 477–493. Springer, 2022. 3, 5, 6
- [19] Danila Rukhovich, Anna Vorontsova, and Anton Konushin. Tr3d: Towards real-time indoor 3d object detection. In *IEEE International Conference on Image Processing (ICIP)*, 2023. 3, 5, 6
- [20] Yichao Shen, Zigang Geng, Yuhui Yuan, Yutong Lin, Ze Liu, Chunyu Wang, Han Hu, Nanning Zheng, and Baining Guo. V-detr: Detr with vertex relative position encoding for 3d object detection. *arXiv preprint arXiv:2308.04409*, 2023. 3, 6
- [21] Xuepeng Shi, Qi Ye, Xiaozhi Chen, Chuangrong Chen, Zhixiang Chen, and Tae-Kyun Kim. Geometry-based distance decomposition for monocular 3d object detection. In *2021 IEEE/CVF International Conference on Computer Vision (ICCV)*, pages 15152–15161, 2021. 1
- [22] Shuran Song and Jianxiong Xiao. Deep sliding shapes for amodal 3d object detection in rgb-d images. In *Proceedings of the IEEE conference on computer vision and pattern recognition*, pages 808–816, 2016. 3
- [23] Shuran Song, Samuel P. Lichtenberg, and Jianxiong Xiao. Sun rgb-d: A rgb-d scene understanding benchmark suite. In *Proceedings of the IEEE Computer Society Conference on Computer Vision and Pattern Recognition*, pages 567–576. IEEE Computer Society, 2015. 3, 5
- [24] Haiyang Wang, Lihe Ding, Shaocong Dong, Shaoshuai Shi, Aoxue Li, Jianan Li, Zhenguo Li, and Liwei Wang. CA-Group3d: Class-aware grouping for 3d object detection on point clouds. In *Advances in Neural Information Processing Systems*, 2022. 3, 6
- [25] Yikai Wang, Xinghao Chen, Lele Cao, Wenbing Huang, Fuchun Sun, and Yunhe Wang. Multimodal token fusion for vision transformers. In *IEEE Conference on Computer Vision and Pattern Recognition (CVPR)*, 2022. 3, 6

- [26] Zhenyu Wang, Ya-Li Li, Xi Chen, Hengshuang Zhao, and Shengjin Wang. Uni3detr: Unified 3d detection transformer. *Advances in Neural Information Processing Systems*, 36: 39876–39896, 2023. [6](#)
- [27] Hao Yang, Chen Shi, Yihong Chen, and Liwei Wang. Boosting 3d object detection via object-focused image fusion. *arXiv preprint arXiv:2207.10589*, 2022. [1](#), [3](#)
- [28] Yu-Qi Yang, Yu-Xiao Guo, Jian-Yu Xiong, Yang Liu, Hao Pan, Peng-Shuai Wang, Xin Tong, and Baining Guo. Swin3d: A pretrained transformer backbone for 3d indoor scene understanding. *Computational Visual Media*, 11(1): 83–101, 2025. [7](#)
- [29] Yun Zhu, Le Hui, Yaqi Shen, and Jin Xie. Spgroup3d: Superpoint grouping network for indoor 3d object detection. In *Proceedings of the AAAI Conference on Artificial Intelligence*, pages 7811–7819, 2024. [3](#), [6](#)